

# Using Lithium and Beryllium to Study Structure and Evolution of Rotating Stars

WUMING YANG,<sup>1</sup> HAIBO YUAN,<sup>1,2</sup> YAQIAN WU,<sup>3</sup> SHAOLAN BI,<sup>1,2</sup> AND ZHIJIA TIAN<sup>4</sup>

<sup>1</sup>*School of Physics and Astronomy, Beijing Normal University, Beijing 100875, China.*

<sup>2</sup>*Institute for Frontiers in Astronomy and Astrophysics, Beijing Normal University, Beijing, China.*

<sup>3</sup>*Key Laboratory of Optical Astronomy, National Astronomical Observatories, Chinese Academy of Sciences, A20 Datun Road, Chaoyang District, Beijing, 100101, China.*

<sup>4</sup>*Department of Astronomy, Key Laboratory of Astroparticle Physics of Yunnan Province, Yunnan University, Kunming 650200, China.*

## ABSTRACT

The chemical composition of the Sun is still a highly controversial issue. No solar model has yet been able to simultaneously reproduce the solar lithium and beryllium abundances, along with helioseismic results, including the rotation profile. Lithium and beryllium are fragile elements that are highly sensitive to the physical conditions, as well as to transport and mixing processes within and below the convective zone (CZ). Uncovering the transport mechanisms responsible for the depletion of Li and Be in the Sun is crucial for using them as tools to understand stellar interiors and the associated transport and mixing processes. We constructed rotating solar models based on Magg's abundance scale, incorporating the effects of convective overshoot and magnetic fields. The rotating model exhibits superior sound speed and density profile and successfully reproduces the observed ratios  $r_{02}$  and  $r_{13}$ . It also matches the seismically inferred CZ depth, surface helium abundance, and rotation profile, as well as the detected Li and Be abundances and neutrino fluxes within  $1\sigma$ . The depletion of Li is dominated by convective overshoot and rotational mixing, while Be depletion is primarily driven by gravitational settling and rotational mixing. The presence of the tachocline accelerates Li depletion but slows down Be depletion. These distinct depletion mechanisms result in the surface abundances of Li and Be evolving differently over time.

*Keywords:* Solar abundances; Helioseismology; Solar interior; Solar neutrinos; Stellar evolution; Stellar rotation

## 1. INTRODUCTION

Recent analyses infer that lithium (Li) abundance,  $A(\text{Li})$ , in the solar photosphere and thus the convection zone (CZ) is  $0.96 \pm 0.05$  dex (E. X. Wang et al. 2021), while beryllium (Be)

abundance,  $A(\text{Be})$ , is  $1.32 \pm 0.05$  dex (J. Carlberg et al 2018; S. Korotin & A. Kućinskas 2022), where  $A(x) = \log(N_x/N_H) + 12.0$ . However, at the time of the birth of the Sun, the Li and Be abundances were  $A(\text{Li}) = 3.3$  dex, as derived from meteorites (K. Lodders 2021), and  $A(\text{Be}) = 1.44$  dex, as determined from solar ob-

servations with some corrections (M. Asplund et al. 2021), respectively.

Since J. L. Greenstein & R. S. Richardson (1951) and J. L. Greenstein & E. Tandberg Hansen (1954) first measured the abundances of Li and Be in the solar photosphere, astronomers have recognized that the solar Li is significantly depleted, whereas Be almost remains unchanged (though see Y. Chmielewski et al. (1975) and S. C. Balachandran & R. A. Bell (1998) for further discussions). This phenomenon is commonly referred to as solar lithium depletion.

The elements  ${}^7\text{Li}$  and  ${}^9\text{Be}$  are easily destroyed by energetic proton at temperatures near  $2.5 \times 10^6$  K and  $3.5 \times 10^6$  K, respectively, making them fragile elements. Thus,  ${}^7\text{Li}$  and  ${}^9\text{Be}$  primarily survive in the outer regions of stars with temperature  $T \lesssim 2.3 \times 10^6$  K and  $T \lesssim 3.0 \times 10^6$  K, respectively. The depth of the Sun's CZ can be measured using helioseismology. The inferred radius of the base of the CZ (BCZ),  $r_{cz}$ , is  $0.713 \pm 0.003R_{\odot}$  (J. Christensen-Dalsgaard et al. 1991) or  $0.713 \pm 0.001R_{\odot}$  (S. Basu & H. M. Antia 1997). The Sun's rotation profile can also be determined via helioseismology (M. J. Thompson et al. 2003; A. Eff-Darwich et al. 2008). Solar models predict that the temperature at the BCZ is about  $(2.20 \pm 0.04) \times 10^6$  K (W. Yang & Z. Tian 2024). Therefore, the convection in the present Sun cannot account for the depletion of Li and Be in the CZ. This indicates that a mixing mechanism must be operating in the solar radiative region, especially below the CZ, to transport Li and Be from the BCZ into a higher-temperature region where they are burned. Thus, Li and Be abundances provide valuable insights into the interiors of stars and physical processes occurring within them. Both Li and Be are excellent astrophysical tracers of transport and mixing processes within and below the CZ of solar-type stars.

To better understand stellar interiors and the mechanisms behind Li and Be depletion, the

abundances of these elements have been measured in many solar twins and solar-type stars (R. Smiljanic et al. 2011; Y. Takeda et al. 2011; M. C. Gálvez-Ortiz et al. 2011; M. Carlos et al 2019, 2020; A. M. Boesgaard et al. 2020, 2022). The Li abundances of other late-type stars have also been determined (M. Y. Ding et al. 2024; E. X. Wang et al. 2024). With  $A(\text{Li})_{\odot} = 1.07_{-0.02}^{+0.03}$  dex, M. Carlos et al (2019) found that the Sun has the lowest Li abundance compared to solar twins at a similar age. A. M. Boesgaard et al. (2020, 2022) obtained similar results, showing that Sun's  $A(\text{Li})$  falls within the lower third of their total sample of solar-mass stars, whereas  $A(\text{Be})$  is in the upper third. This suggests that Li and Be depletion may arise from different physical mechanisms. The Sun appears to be exceptionally depleted in Li but only slightly depleted in Be. These characteristics provide strong constraints on the transport and mixing mechanisms below the CZ, as well as their efficiencies.

Many stellar models incorporating different physics have been used to explain the Li depletion of the Sun and solar-like stars. For example, C. Charbonnel & S. Talon (2005) considered the effects of gravity waves; D. R. Xiong & L. Deng (2009) accounted for overshooting and gravitational settling; while rotation and diffusion were included in the models of J. D. Do Nascimento et al. (2009), T. Dumont et al. (2021a,b), T. Constantino et al. (2021), P. Eggenberger et al. (2022), and W. Yang & Z. Tian (2024). The solar Li abundance alone can be easily reproduced by an evolutionary model. However, simultaneously matching the observed Li, Be, and other solar characteristics remains challenging. For instance, the rotating model of P. Eggenberger et al. (2022) successfully reproduces the He and Li abundances, as well as the rotation profile of the Sun, but fails to match the observed Be abundance, the seismically inferred CZ depth, and the sound speed profile.

This highlights the complexity of solar modeling.

Moreover, the chemical composition of the Sun remains a highly debated issue (M. Asplund et al. 2021; E. Magg et al. 2022; A. G. M. Pietrow et al. 2023; W. Yang & Z. Tian 2024, and references therein). To replicate the solar structure and element abundances, the effects of various accretion processes have been considered (Q. S. Zhang et al. 2019; M. Kunitomo et al. 2022). Rotational mixing has been proposed as a solution to the low helium abundance problem in solar models based on recently estimated solar metallicity (W. M. Yang & S. L. Bi 2007; W. Yang 2016, 2019, 2022; W. Yang & Z. Tian 2024). However, there is no direct evidence that rotational mixing increases the Sun’s surface helium abundance. Mechanisms that transport material into the Sun’s radiative region would also carry helium-rich material from the radiative region to the CZ, potentially enhancing the surface helium abundance. If these mechanisms are driven by rotation, then a rotating solar model should be able to simultaneously reproduce the observed surface Li and Be abundances, the seismically inferred surface helium abundance, CZ depth, and rotation profile, as well as the surface rotation history speculated from solar-type main-sequence (MS) stars in clusters. In this scenario, the depletion of Li and Be would serve as evidence that rotation enhances surface helium abundance. Thus, obtaining an accurate solar model is crucial for addressing the solar composition problem (or solar modeling problem).

The entire problem of the abundances of Li and Be in the Sun, which has puzzled astronomers for over six decades, requires further close scrutiny. It is imperative to uncover transport mechanisms responsible for the depletion of Li and Be in the Sun in order to use these elements as tracers for understanding stellar interiors and the processes of transport and mixing

within them. Furthermore, a full understanding of Li depletion also aids in accurately determining the primordial Li abundance from observations of the Galaxy’s oldest metal-poor stars. In this study, we present rotating solar models that can simultaneously reproduce the observed Li and Be abundances of the Sun, the seismically inferred rotation profile, and other key characteristics. Our findings demonstrate that the depletion of Li and Be is dominated by different mechanisms. The paper is organized as follows. Input physics are presented in Section 2, calculation results are shown in Section 3, and the results are discussed and summarized in Section 4.

## 2. INPUT PHYSICS

Stellar evolutionary models were computed using the Yale Rotating Stellar Evolution Code (A. S. Endal & S. Sofia 1976; M. H. Pinsonneault et al. 1989; W. M. Yang & S. L. Bi 2007; W. Yang 2016) in its rotation and nonrotation configurations. The OPAL equation-of-state (EOS2005) tables (F. Rogers & A. Nayfonov 2002) and the Opacity Project (OP) (M. J. Seaton 1987; N. R. Badnell et al. 2005) or OPAL (C. Iglesias & F. J. Rogers 1996) opacity tables were utilized, supplemented by the J. W. Ferguson et al. (2005) opacity tables at a low temperature. These tables were reconstructed with E. Magg et al. (2022) mixtures. The Roseland mean opacity between  $\log T = 4.1$  and 4.0 was determined through linear interpolation of the two opacity tables. The nuclear reaction rates were calculated using the subroutine of J. N. Bahcall & M. H. Pinsonneault (1992), updated by J. N. Bahcall et al. (1995, 2001) and W. Yang & Z. Tian (2024). The nuclear reaction rates of Li and Be as a function of temperature were calculated for temperatures exceeding  $10^6$  K, under the assumption that Li and Be are completely destroyed at  $T \geq 10^7$  K. The diffusion and settling of both helium and heavy elements were computed using the diffusion coeffi-

cients of [A. A. Thoul et al. \(1994\)](#). The effects of radiative levitation on chemical transport were not incorporated into our models. The radiative effects can cause the abundance and mixture of the heavy elements to vary with stellar age and position in the Sun ([S. Turcotte et al. 1998](#)). However, the impact of radiative acceleration may be mitigated by the effects of rotation and magnetic fields.

Li and Be abundances are generally not included in the metal abundance  $Z$  because their concentrations are too low. Similarly, the diffusion and settling of heavy elements do not account for Li and Be. However, in this work, we incorporated the diffusion and settling of Li and Be into all models.

In the atmosphere, the [K. S. Krishna Swamy \(1966\)](#)  $T - \tau$  relation was adopted. The boundary of the CZ was calculated using the Schwarzschild criterion, and energy transfer by convection was treated according to the standard mixing-length theory ([E. Böhm-Vitense 1958](#)). The depth of the overshoot region was given by  $\delta_{\text{ov}} H_p$ , where  $\delta_{\text{ov}}$  is a free parameter, and  $H_p$  is the local pressure scale height. The overshoot region was assumed to be both fully mixed and adiabatically stratified.

The angular momentum loss from the CZ due to magnetic braking was computed using Kawaler's relation ([S. D. Kawaler 1988](#); [B. Chaboyer et al 1995](#)). The redistributions of angular momentum and chemical compositions were treated as a diffusion process ([A. S. Endal & S. Sofia 1978](#); [W. Yang 2016](#)), i.e.,

$$\frac{\partial \Omega}{\partial t} = \frac{1}{\rho r^4} \frac{\partial}{\partial r} [(\rho r^4 (f_\Omega D_r + f_m D_m) \frac{\partial \Omega}{\partial r})] \quad (1)$$

for angular momentum transport and

$$\begin{aligned} \frac{\partial X_i}{\partial t} = & \frac{1}{\rho r^2} \frac{\partial}{\partial r} [\rho r^2 (f_c f_\Omega D_r + f_{cm} f_m D_m) \frac{\partial X_i}{\partial r}] \\ & + (\frac{\partial X_i}{\partial t})_{\text{nuc}} - \frac{1}{\rho r^2} \frac{\partial}{\partial r} (\rho r^2 X_i V_i) \end{aligned} \quad (2)$$

for the change in the mass fraction  $X_i$  of chemical species  $i$ , where  $D_r$  is the diffusion coefficient

caused by rotational instabilities, including the dynamical instabilities described in [A. S. Endal & S. Sofia \(1978\)](#) and [M. H. Pinsonneault et al. \(1989\)](#), as well as the secular shear instability

$$D = \frac{2c}{27G} \left| \frac{d \ln T}{dr} - \frac{2}{3} \frac{d \ln \rho}{dr} \right|^{-1} \frac{r^4}{\kappa \rho M(r)} \left( \frac{d\Omega}{dr} \right)^2 \quad (3)$$

of [J. P. Zahn \(1993\)](#);  $\rho$  is the density; and  $V_i$  is the velocity of microscopic diffusion and settling given by [A. A. Thoul et al. \(1994\)](#);  $\kappa$  is the opacity;  $c$  and  $G$  are the light velocity and gravitational constant, respectively. The diffusion coefficient due to magnetic fields,  $D_m$ , is defined by ([W. M. Yang & S. L. Bi 2006](#))

$$D_m = r^2 \Omega \frac{B_r^2}{B^2}. \quad (4)$$

We use the radial ( $B_r$ ) and toroidal ( $B_t$ ) components to express a magnetic field vector  $\mathbf{B} = (B_r, B_t)$ . Given that  $|B_t| \gg |B_r|$ , here, we take  $|B| \approx |B_t|$ . The magnetic field compositions  $|B_r|$  and  $|B_t|$  are calculated using Equations (22) and (23) of [H. C. Spruit \(2002\)](#). The parameters  $f_\Omega$  and  $f_m$  were introduced to represent some inherent uncertainties in the diffusion equation, while the parameters  $f_c$  and  $f_{cm}$  were used to account for how the instabilities and magnetic fields mix material less efficiently than they transport angular momentum ([M. H. Pinsonneault et al. 1989](#); [W. Yang 2016](#)). The default values of  $f_\Omega$  and  $f_c$  are 1 and 0.03, respectively.

All solar models are calibrated to the present solar luminosity  $3.844 \times 10^{33}$  erg s<sup>-1</sup>, radius  $6.9598 \times 10^{10}$  cm, mass  $1.9891 \times 10^{33}$  g, and age 4.57 Gyr ([J. N. Bahcall et al. 1995](#)). The initial hydrogen abundance  $X_0$ , metal abundance  $Z_0$ , and mixing-length parameter  $\alpha_{\text{MLT}}$  are free parameters adjusted to match the constraints of luminosity and radius around  $10^{-5}$  and an observed  $(Z/X)_s$ . The initial helium abundance is determined by  $Y_0 = 1 - X_0 - Z_0$ . The initial rotation rate,  $\Omega_i$ , of rotating models is also a free parameter.

We constructed the following five models: (1) MBS22, a standard solar model (SSM) constructed using OP opacity tables with [E. Magg et al. \(2022\)](#) mixture; (2) MBS22r1, a rotating model that includes the effects of magnetic fields ([W. Yang 2016](#)) and is constructed using OPAL opacity tables with the [E. Magg et al. \(2022\)](#) mixture; (3) MBS22r2 and MBS22r3, which are similar to MBS22r1 but have higher mixing efficiency; (4) MBS22rt, similar to MBS22r2 but with an assumed tachocline of  $0.05R$  and a different mixing efficiency within the tachocline, where  $R$  represents the stellar radius. The four rotating models share the same  $f_m$  but have different  $f_{cm}$ . The fundamental parameters of these models are listed in Table 1.

### 3. CALCULATION RESULTS

#### 3.1. Results of Standard Solar Model

The surface Li and Be abundances of MBS22 are 2.45 and 1.30, respectively. The predicted Be abundance is in agreement with the observed value of  $1.32 \pm 0.05$ , but the Li abundance is too high. Moreover, the CZ base radius of  $0.718 R_\odot$  and the surface helium abundance of 0.2406 disagree with the seismically inferred values. The position of the BCZ is too shallow, and the surface helium abundance is too low.

Figure 1 shows that the temperature at the BCZ of non-rotating models as a function of age. The vertical dotted and dashed lines represent the ages at  $T_{bcz} = 3.5 \times 10^6$  and  $2.5 \times 10^6$  K, respectively. (b), (c) Surface lithium and beryllium abundances as a function of age for different solar models. The age of the solar models at the zero-age main sequence (ZAMS) is about 40 Myr. The scatter symbols refer to estimated Li or Be abundance ([A. M. Boesgaard et al. 2003a,b, 2004, 2022](#); [M. C. Gálvez-Ortiz et al. 2011](#); [M. Carlos et al 2019](#); [E. X. Wang et al. 2021](#); [S. Korotin & A. Kučinskás 2022](#)).

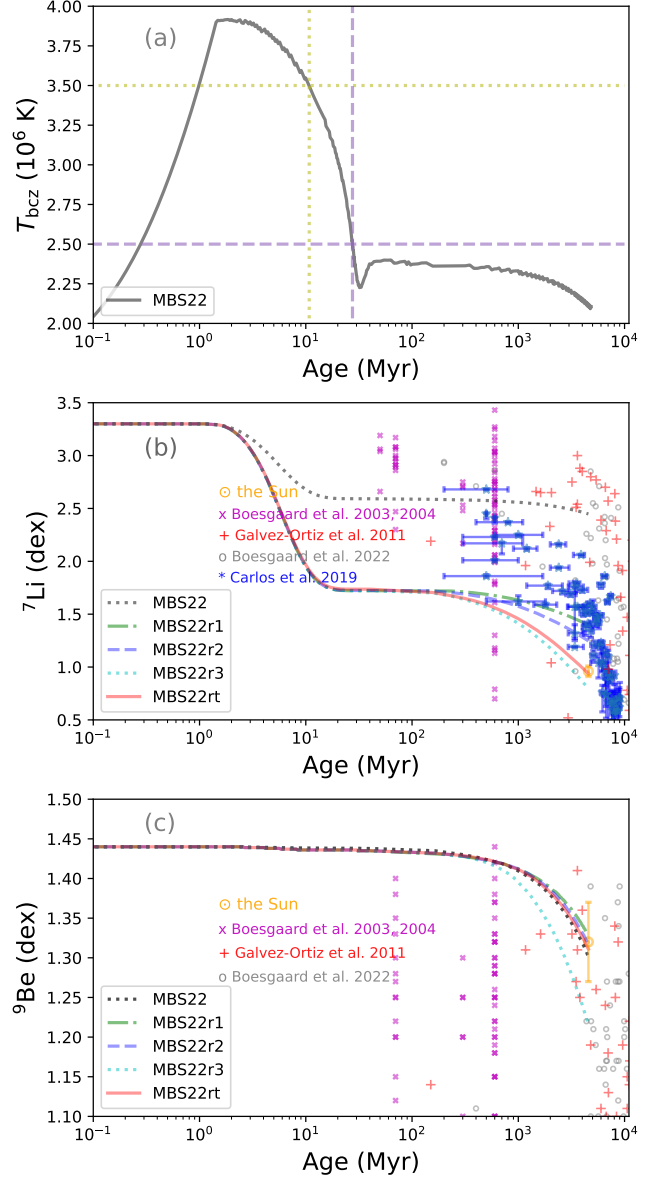


**Figure 1.** (a) Temperature at the BCZ of non-rotating models as a function of age. The vertical dotted and dashed lines represent the ages at  $T_{bcz} = 3.5 \times 10^6$  and  $2.5 \times 10^6$  K, respectively. (b), (c) Surface lithium and beryllium abundances as a function of age for different solar models. The age of the solar models at the zero-age main sequence (ZAMS) is about 40 Myr. The scatter symbols refer to estimated Li or Be abundance ([A. M. Boesgaard et al. 2003a,b, 2004, 2022](#); [M. C. Gálvez-Ortiz et al. 2011](#); [M. Carlos et al 2019](#); [E. X. Wang et al. 2021](#); [S. Korotin & A. Kučinskás 2022](#)).



**Table 1.** Fundamental Parameters of Models.

Model	$Y_0$	$Z_0$	$\alpha_{\text{MLT}}$	$\delta_{\text{ov}}$	$r_{\text{cz}}$	$T_{\text{bcz}}$	$Y_s$	$Z_s$	$(Z/X)_s$	$\Omega_z$	$f_m$	$f_{cm}$	$A(\text{Li})_s$	$A(\text{Be})_s$
MBS22	0.27066	0.0183	2.0973	0	0.718	2.12	0.2406	0.01646	0.0222	0	...	...	2.45	1.30
MBS22r1	0.27392	0.0184	2.0755	0.09	0.711	2.21	0.2486	0.01638	0.0223	$\sim 10$	1	1	1.40	1.33
MBS22r2	0.27391	0.0184	2.0691	0.09	0.713	2.20	0.2500	0.01640	0.0223	$\sim 10$	1	2	1.25	1.32
MBS22r3	0.27391	0.0184	2.0556	0.09	0.713	2.20	0.2529	0.01641	0.0225	$\sim 10$	1	6	0.82	1.22
MBS22rt	0.27391	0.0184	2.0613	0.09	0.713	2.20	0.2517	0.01641	0.0224	$\sim 10$	1	2 <sup>a</sup>	0.94	1.31

Notes. The CZ radius  $r_{\text{cz}}$ , CZ temperature  $T_{\text{bcz}}$ , angular velocity  $\Omega_z$ ,  $f_m$ , and  $f_{cm}$  are in units of  $R_\odot$ ,  $10^6$  K,  $10^{-6}$  rad  $\text{s}^{-1}$ ,  $10^{-4}$ , and  $10^{-4}$ , respectively. <sup>a</sup> The value of  $f_{cm}$  within the tachocline of MBS22rt is 0.0005.

age due to the effects of convection (see Figure 1).

During the MS stage, the temperature  $T_{\text{bcz}}$  does not exceed  $2.4 \times 10^6$  K (see Figure 1). Since the burning rates of  ${}^7\text{Li}$  and  ${}^9\text{Be}$  in the CZ of MBS22 are low and decrease rapidly with a decrease in temperature ( $\partial \ln A(\text{Li})/\partial t < 4 \times 10^{-18}$   $\text{s}^{-1}$  and  $\partial \ln A(\text{Be})/\partial t < 2 \times 10^{-21}$   $\text{s}^{-1}$ ; see Figure 2), their burning in the CZ is insufficient to significantly alter their abundances. The changes in the surface Li and Be abundances of MBS22 during this stage are primarily due to gravitational settling rather than nuclear fusion reactions in the CZ. Gravitational settling is the dominant mechanism affecting the surface Be abundance. To accurately understand the behavior of Li and Be, the effects of gravitational settling must be considered. If gravitational settling were neglected, the surface Li and Be abundances would remain unchanged during the MS stage of SSMs.

From MBS22, it is evident that the seismically inferred CZ depth, surface He abundance, and Li abundance do not support the SSM. Additional mixing mechanisms, such as rotational effects, are required to simultaneously explain the solar Li and Be depletion, as well as other observed characteristics.

### 3.2. Results of Rotating Models

To reproduce the observed Li abundance and other characteristics, we considered the effects

of rotation, including magnetic fields (W. Yang 2016), and constructed four rotating models with different mixing efficiencies. In these models, convective overshooting with  $\delta_{\text{ov}} = 0.09$  is necessary to reproduce the seismically inferred CZ depth. Convective overshooting carries material from the CZ into a region of higher temperature. During the pre-MS stage, convection and overshooting predominantly influence the change in the Sun's surface Li abundance, as the temperature  $T_{\text{bcz}}$  during this stage is high enough to rapidly destroy Li (see Figure 1). However, these processes have little effect on the surface Be abundance and the Li abundance during the MS stage.

The effects of convective overshooting alone cannot explain solar Li depletion unless we ignore the constraints from helioseismology, such as the seismically inferred CZ depth and the observed frequency separation ratios  $r_{02}$  and  $r_{13}$  that are influenced by the acoustic depth of the CZ (I. W. Roxburgh & S. V. Vorontsov 2003), and adopt a larger  $\delta_{\text{ov}}$ . During the MS stage, changes in surface Li and Be abundances in rotating models are driven by magnetic and hydrodynamic mixing, alongside gravitational settling.

In the nonrotating model, Li from the CZ that settles near the top of the radiative region does not accumulate there because the temperature is high enough to destroy it, and diffusion re-

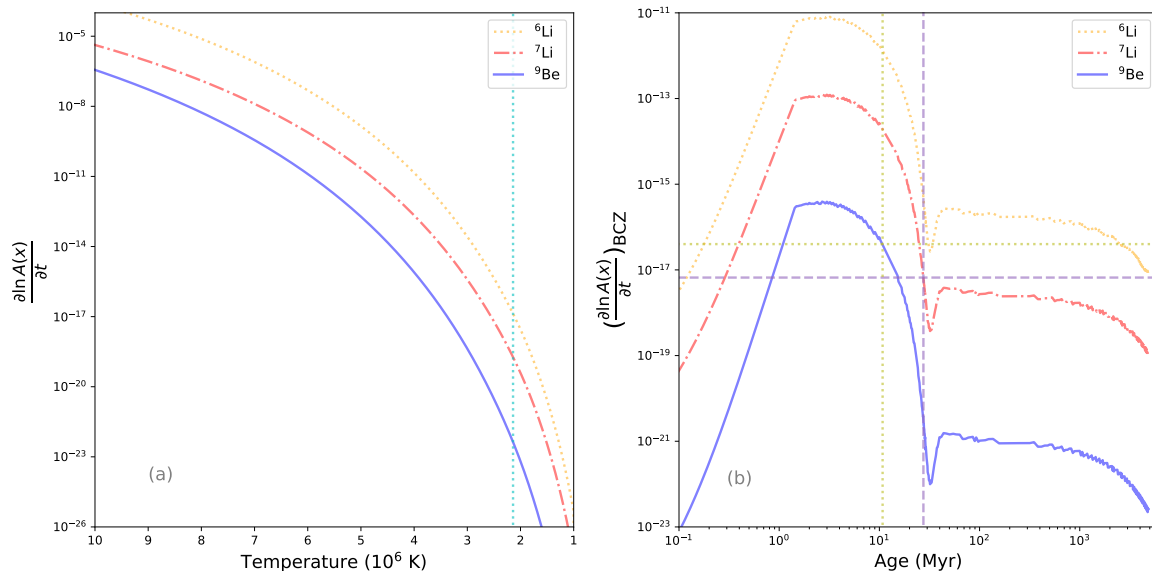


**Figure 2.** (a) Burning rates of  ${}^6\text{Li}$ ,  ${}^7\text{Li}$ , and  ${}^9\text{Be}$  of MBS22 as a function of temperature. The vertical dotted line represents the BCZ temperature. (b) Burning rates of  ${}^6\text{Li}$ ,  ${}^7\text{Li}$ , and  ${}^9\text{Be}$  at BCZ as a function of age. The vertical dotted and dashed lines represent the ages at  $T_{\text{bcz}} = 3.5 \times 10^6$  and  $2.5 \times 10^6$  K, respectively.

moves it. However, Be from the CZ can partially accumulate in that region since the temperature is not high enough to effectively burn it, and diffusion only removes a fraction of the Be. As a result, Li and Be exhibit different distribution profiles (see the black dotted lines in Figure 3).

In rotating models, rotational mixing transports Li and Be to regions with higher temperatures (see Figure 3), where they are burned more rapidly. When Li from the CZ is brought into the radiative region, helium from the radiative region can be transported to the CZ. This process leads to an increase in surface helium abundance. Therefore, in a rotating star, surface Li depletion and He enhancement occur simultaneously. If the efficiency of rotational mixing is too high, it will result in surface Li and Be abundances being too low, while the surface He abundance becomes excessively high.

With  $f_m = 0.0001$  and  $f_{cm} = 0.0001$ , we constructed the rotating model MBS22r1. The surface He, Li, and Be abundances predicted by MBS22r1 for the Sun are 0.2486, 1.40, and 1.33

dex, respectively. The surface He and Be abundances are consistent with inferred values; however, the surface Li abundance is too high.

With  $f_{cm} = 0.0002$ , we constructed the rotating model MBS22r2. This model has better sound speed and density profiles than SSM MBS22 and reproduces the observed ratios  $r_{02}$  and  $r_{13}$  (see Figure 4). The surface helium abundance of 0.2500 and the CZ base radius of  $0.713 R_{\odot}$  of MBS22r2 are in good agreement with the seismically inferred values. The surface Be abundance of 1.32 dex matches the  $1.32 \pm 0.05$  dex determined by S. Korotin & A. Kučinskas (2022). However, the surface Li abundance of 1.25 dex remains higher than the  $1.04 \pm 0.10$  dex advocated by K. Lodders (2021) or the 0.96 dex reported by E. X. Wang et al. (2021).

Models MBS22r1 and MBS22r2 show that surface He abundance increases while Li abundance decreases with higher mixing efficiency. However, the surface Li abundances in both models remain higher than the observed value, suggesting that the mixing efficiency may be under-

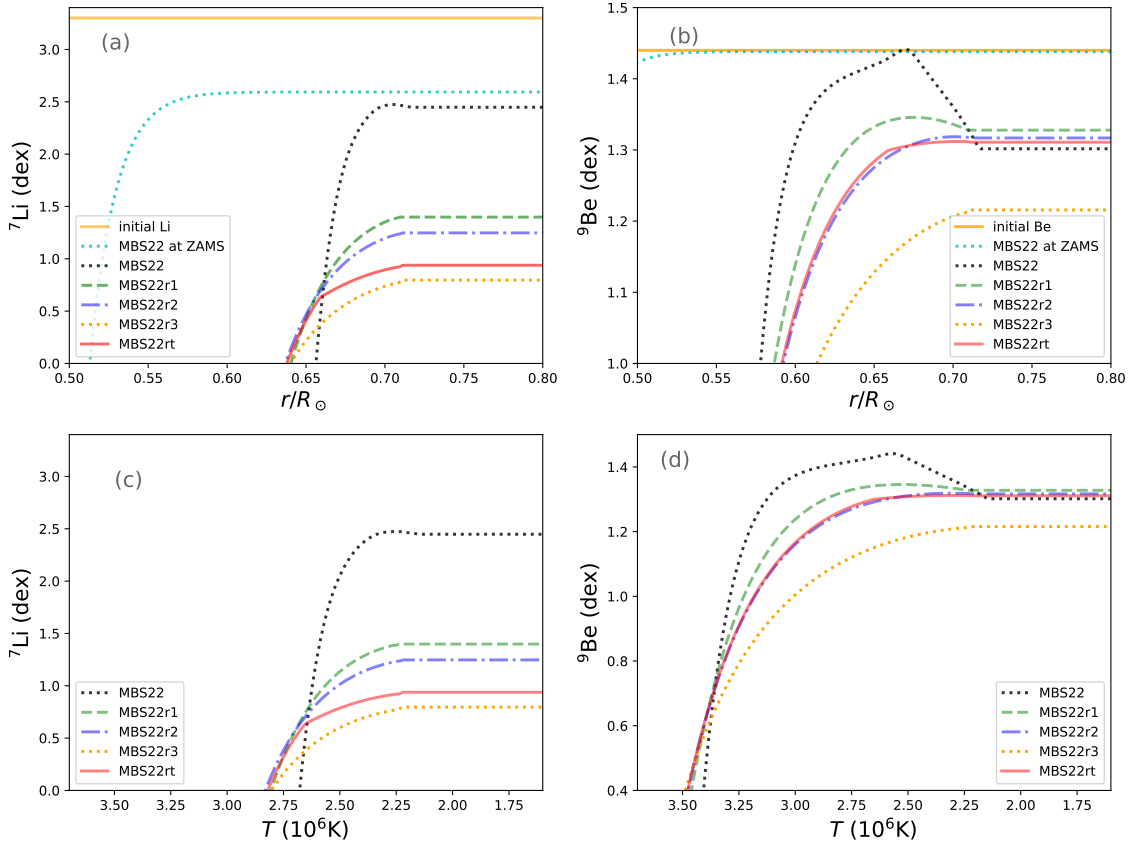


**Figure 3.** (a), (b) Lithium and beryllium profiles as a function of radius for different models. (c), (d) Lithium and beryllium profiles as a function of temperature for different models.

estimated. Thus, we constructed the rotating model MBS22r3 with  $f_{cm} = 0.0006$ . The surface He, Li, and Be abundances predicted by MBS22r3 for the Sun are 0.2529, 0.82 dex, and 1.22 dex, respectively. The surface He abundance is higher than the value inferred from helioseismology, while the surface Li and Be abundances are lower than the observed values, indicating that MBS22r3 likely overestimates the Sun’s mixing efficiency.

Moreover, we also constructed a rotating model with  $f_{cm} = 0.0004$ . The surface Li and Be abundances predicted by this model for the Sun are 1.03 and 1.27 dex, respectively. When adopting the Li abundance of  $0.96 \pm 0.05$  dex

advocated by E. X. Wang et al. (2021) and the Be abundance of 1.32 dex to constrain solar models, it becomes apparent that this model underestimates the mixing of Li while overestimating that of Be. Helioseismology has shown that the Sun has a tachocline with a width of  $0.039 \pm 0.013 R_\odot$  below the CZ (P. Charbonneau et al. 1999), where latitudinal differential rotation occurs. The shear in the tachocline is expected to be very strong; therefore, a component associated with the hydrodynamical transport of material should be present. Consequently, it is widely believed that rotational mixing is more efficient in the tachocline than in other regions.



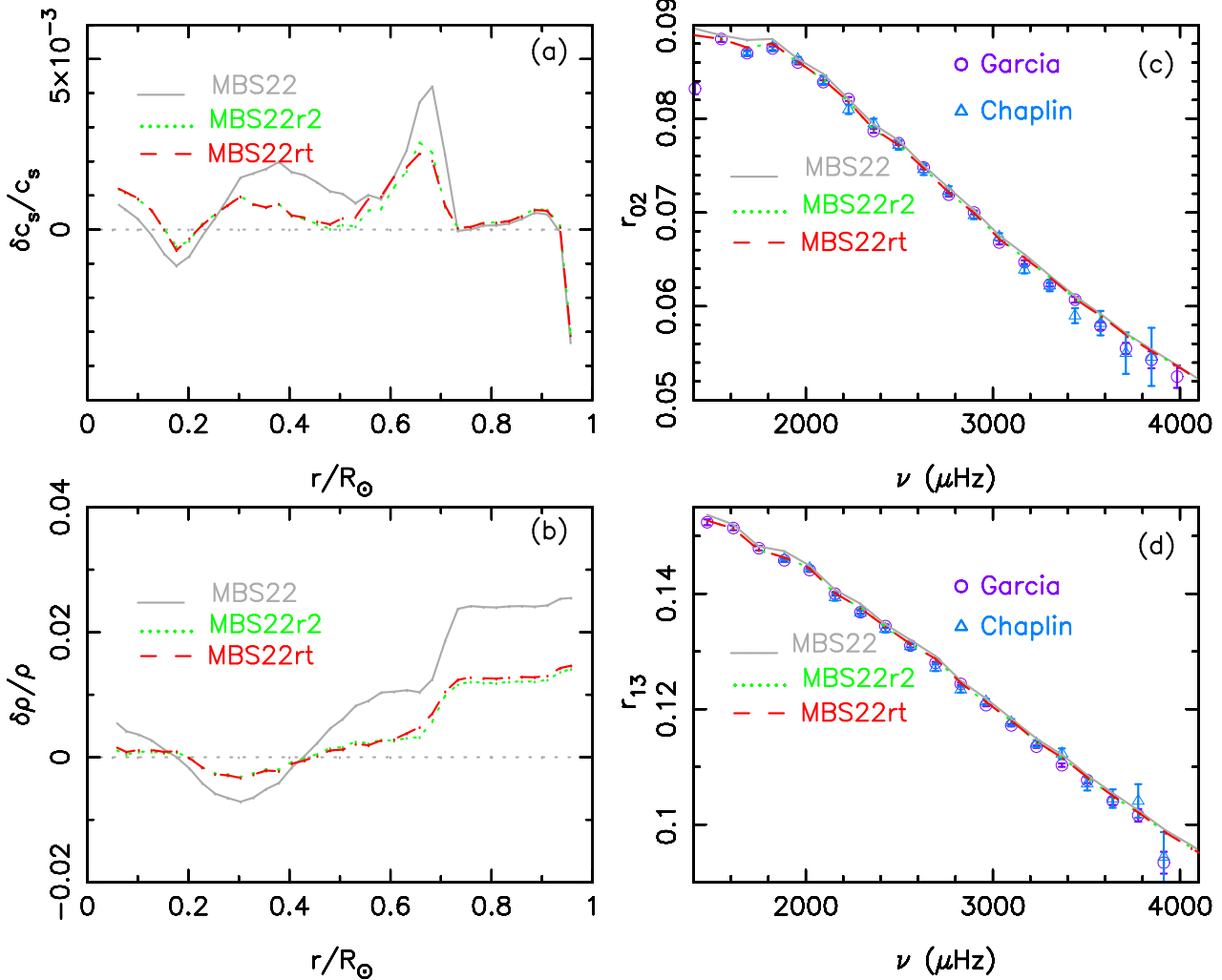


**Figure 4.** (a), (b) Relative sound speed and density differences, in the sense (Sun-Model)/Model, between the Sun and models. The inferred sound speed and density of the Sun are given by *S. Basu et al. (2009)*. (c), (d) Distributions of observed and predicted ratios  $r_{02}$  and  $r_{13}$  as a function of frequency, which are calculated by using smooth five-point separations of *I. W. Roxburgh & S. V. Vorontsov (2003)*. The circles and triangles show the ratios calculated from the frequencies observed by GOLF and VIRGO (*R. A. García et al. 2011*) and by BiSON (*W. J. Chaplin et al. 1999*), respectively.

Assuming that the width of the tachocline is  $0.05R$  and the mixing is more efficient in tachocline than in other regions, we achieved this by setting  $f_{cm} = 0.0005$  and  $f_c = 0.03 \times 2.5$  in the tachocline, while using  $f_{cm} = 0.0002$  and  $f_c = 0.03$  in other regions. With these assumptions, we constructed the model MBS22rt. The surface helium abundance of 0.2517 and the CZ base radius of  $0.713 R_\odot$  for MBS22rt are in good agreement with the seismically inferred values. It also exhibits superior sound speed and den-

sity profiles compared to MBS22 and reproduces the observed ratios  $r_{02}$  and  $r_{13}$  (see Figure 4). Additionally, the surface Li abundance of 0.94 dex in MBS22rt agrees with the  $0.96 \pm 0.05$  dex advocated by *E. X. Wang et al. (2021)*, while the surface Be abundance of 1.31 dex is consistent with the  $1.32 \pm 0.05$  dex reported by *S. Korotin & A. Kučinskas (2022)*.

Table 1 shows that the surface Be abundances in MBS22r1, MBS22r2, and MBS22rt are higher, whereas that in MBS22r3 is lower

than the value predicted by MBS22. Panel (b) of Figure 3 illustrates that the Be abundance below the CZ in MBS22r1 exceeds that within the CZ. The temperature at the base of tachocline of a solar model is about  $2.6 \times 10^6$  K, which is insufficient to effectively destroy beryllium. Gravitational settling causes the Be abundance in the CZ to accumulate in the region below it, resulting in a lower Be abundance within the CZ compared to the region beneath it. When the rotational mixing efficiency is low, Be below the CZ cannot be efficiently transported to higher-temperature regions where it would be burned. In such cases, the negative Be abundance gradient causes rotational mixing below the CZ to partially counteract the effect of gravitational settling. Consequently, the surface Be abundance of a rotating model with low mixing efficiency is higher than that of a nonrotating model.

However, when the mixing efficiency is high, as in MBS22r3, Be below the CZ is rapidly transported to higher-temperature regions and burned. This results in a positive Be abundance gradient below the CZ (see Figure 3), with rotational mixing transporting Be from the CZ to regions where it is destroyed. Consequently, the surface Be abundance in a high-efficiency rotating model is lower than that in a nonrotating model. The Sun’s surface Be abundance is influenced by gravitational settling, rotational mixing, and the tachocline. Unlike Be, the temperature in the tachocline is sufficient to effectively destroy Li, leading to different behavior for these elements.

Our calculations show that the upper limit of the surface Be abundance predicted by rotating models is 1.34 dex, determined by the interaction between gravitational settling and rotational mixing. Accurately and precisely determining the Sun’s Be abundance is crucial for understanding these processes and their interac-

tions. Be serves as an excellent tracer of these physical processes.

Moreover, Figure 5 shows that MBS22rt predicts a nearly flat rotation profile in the outer part of the radiative region, with an increase in the rotation rate in the solar core. These results are consistent with the predictions of models by W. Yang (2016) and P. Eggenberger et al. (2019, 2022), as well as with those inferred from helioseismology (M. J. Thompson et al. 2003; R. A. García et al. 2008). Additionally, MBS22rt reproduces the surface rotation rates observed in MS solar-type stars in open clusters.

The tachocline affects the surface abundances of Li and Be in the Sun differently due to the distinct physical properties of these elements; specifically, lithium burns at a lower temperature than beryllium. The temperature at the base of tachocline in MBS22rt is around  $2.6 \times 10^6$  K, which is high enough to destroy Li but not enough to effectively burn Be. The existence of a tachocline makes Li in the CZ more easily depleted. Due to the low mixing efficiency at the base of the tachocline in a low-efficiency rotating model, Be in the tachocline cannot be quickly transported to a higher-temperature region to be burned. Rotational mixing below the CZ partially counteracts the gravitational settling of Be within and below the CZ. Therefore, the presence of the tachocline impedes the depletion of Be but accelerates the depletion of Li. Accurately and precisely determining the Sun’s Be abundance will provide valuable insights into the Sun’s interiors and the physical processes occurring below the CZ.

Moreover, the fluxes of  $pp$ ,  $pep$ ,  $hep$ ,  ${}^7\text{Be}$ , and  ${}^8\text{B}$  neutrinos, as well as the total fluxes of  ${}^{13}\text{N}$ ,  ${}^{15}\text{O}$ , and  ${}^{17}\text{F}$  neutrinos computed from the rotating model MBS22rt, agree with those reported by J. Bergström et al. (2016), Borexino Collaboration (2018), A. Appell et al. (2022),

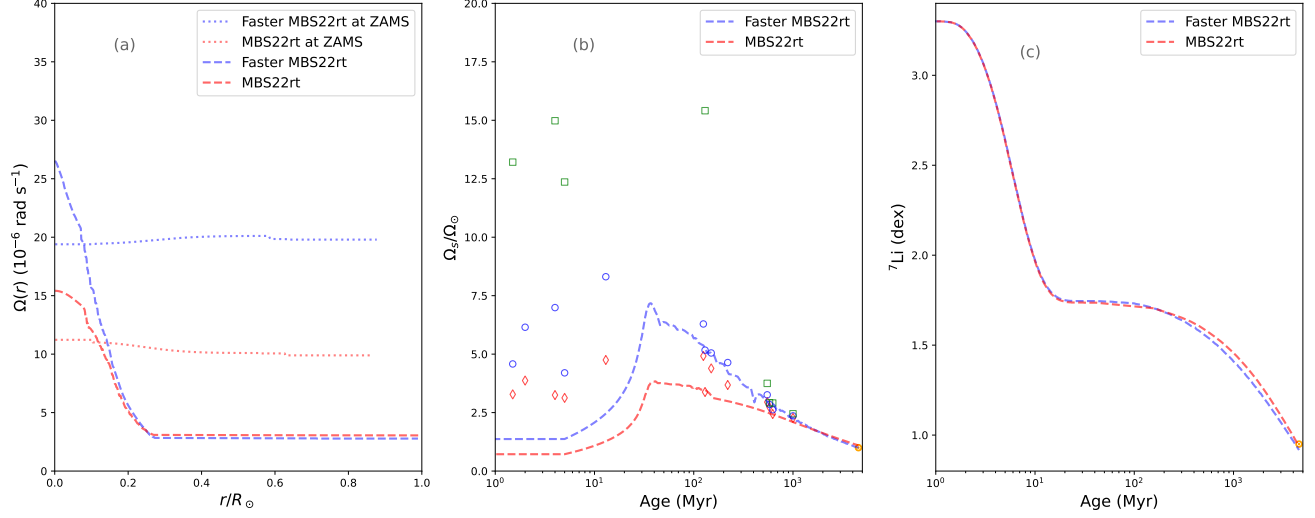


**Figure 5.** (a) Rotation profiles of models at the ZAMS and the age of 4.57 Gyr. The age of the solar models at the ZAMS is about 40 Myr. (b) Surface angular velocity as a function of age for different solar models. Open symbols refer to observations of surface angular velocities in open clusters taken from Table 1 of *F. Gallet & J. Bouvier (2015)*, with green, blue, and red symbols representing the 90th, 50th, and 25th rotational percentiles, respectively. The orange circle in the lower right indicates the surface rotation rate of the Sun. (c) Surface lithium abundances as a function of age for different solar models.

**Table 2.** Measured and Predicted Solar Neutrino Fluxes.

Model	$pp$	$pep$	$hep$	${}^7\text{Be}$	${}^8\text{B}$	${}^{13}\text{N}$	${}^{15}\text{O}$	${}^{17}\text{F}$
Measured	$6.06^{+0.02a}_{-0.06}$	$1.6 \pm 0.3^b$	...	$4.84 \pm 0.24^a$	$5.21 \pm 0.27^c$	...	...	...
B16 <sup>d</sup>	$5.97^{+0.04}_{-0.03}$	$1.448 \pm 0.013$	$19^{+12}_{-9}$	$4.80^{+0.24}_{-0.22}$	$5.16^{+0.13}_{-0.09}$	$\leq 13.7$	$\leq 2.8$	$\leq 85$
Borexino <sup>e</sup>	$6.1 \pm 0.5$	$1.39 \pm 0.19$	$< 220$	$4.99 \pm 0.11$	$5.68^{+0.39}_{-0.41}$	$6.7^{+1.2}_{-0.8}$		
MBS22	5.99	1.446	9.75	4.85	5.25	4.02	2.00	4.86
MBS22r1	5.98	1.445	9.67	4.97	5.55	4.23	2.12	5.16
MBS22r2	5.99	1.446	9.67	4.97	5.55	4.23	2.12	5.16
MBS22r3	5.98	1.442	9.67	4.97	5.55	4.21	2.11	5.14
MBS22rt	5.98	1.444	9.67	4.97	5.55	4.23	2.12	5.16

Notes. The fluxes of  $pp$ ,  $pep$ ,  $hep$ ,  ${}^7\text{Be}$ ,  ${}^8\text{B}$ ,  ${}^{13}\text{N}$ ,  ${}^{15}\text{O}$ , and  ${}^{17}\text{F}$  neutrinos are in units of  $10^{10}$ ,  $10^8$ ,  $10^3$ ,  $10^9$ ,  $10^6$ ,  $10^8$ ,  $10^8$ , and  $10^6 \text{ cm}^{-2} \text{ s}^{-1}$ , respectively.

<sup>a</sup>G. Bellini et al. (2011).

<sup>b</sup>G. Bellini et al. (2012).

<sup>c</sup>S. N. Ahmed et al. (2004).

<sup>d</sup>J. Bergström et al. (2016).

<sup>e</sup>Borexino Collaboration (2018). The total fluxes,  $\Phi(\text{CNO})$ , produced by CNO cycle are given by D. Basilico et al. (2023).

and D. Basilio et al. (2023) at the level of  $1\sigma$  (see Table 2). This indicates that the temperature and density distributions in the nuclear reaction region of the model align with those of the Sun.

## 4. DISCUSSION AND SUMMARY

### 4.1. Discussion

The SSM MBS22 was constructed using OP opacity tables. SSMs constructed with OPAL opacity tables are not as good as those constructed with OP opacity tables (W. Yang & Z. Tian 2024). To reproduce the seismically inferred sound speed and density profile, a linearly increased OPAL opacity and enhanced diffusion, as suggested by W. Yang & Z. Tian (2024), are still necessary. The OPAL opacities used in the rotating models were linearly increased following W. Yang & Z. Tian (2024). Enhanced diffusion results in a higher initial metal abundance and more metals in the radiative region, while leading to a lower metal abundance in the CZ. These effects are similar to those of mass accretion with a variable  $Z$  before the ZAMS (M. Kunitomo & T. Guillot 2021; M. Kunitomo et al. 2022), which may deserve further detailed study in future work, along with the impact of increased opacity. Nevertheless, calculations show that the predicted Li and Be abundances, as well as the rotation profile, are primarily determined by convective overshoot and rotational mixing, including magnetic fields, rather than by these factors.

The isotope  $^6\text{Li}$  was included in this work, but  $^{10}\text{Be}$  was not considered. In our calculations,  $^6\text{Li}$  was completely burned out before the ZAMS, which contradicts observation, as  $^6\text{Li}$  has been detected on the solar surface. Additional mechanisms are necessary to explain the presence of  $^6\text{Li}$ .

Fast rotators in NGC 2264 (J. Bouvier et al. 2016) and the Pleiades (J. Bouvier et al. 2018) have been found to be systematically richer in

Li than their slowly rotating counterparts. P. Eggenberger et al. (2012) found that stars with longer disk-locking periods tend to be more Li depleted, rotate more slowly, and exhibit lower Li abundances at the ZAMS. The timescale of disk-locking of the Sun during the early phase of pre-MS remains unknown.

In our calculations, we assumed a timescale of 5 Myr. For a given disk-locking timescale, models with higher  $\Omega_i$  exhibit higher rotation rates and lower Li abundances at the ZAMS than models with lower  $\Omega_i$  (see Figure 6). For a given initial rotation rate  $\Omega_i$ , models with a shorter disk lifetime tend to have higher Li abundances and rotation rates at the ZAMS compared to those with longer disk-locking phases. These results are consistent with those reported by P. Eggenberger et al. (2012, see their Figures 5 and 8) and J. P. Marques & M. J. Goupil (2013, see their Figure 4.6). For a given low initial rotation rate, the timescale does not significantly affect our results (see Figure 6).

From the birth of a star to its ZAMS, rotating models that include magnetic field effects behave almost like homogenous solid-body rotation models (see Figure 5), except for the distributions of Li and Be, which have been burned out in the center of the models (see Figure 3). The surface rotation rate reaches its maximum value around the ZAMS due to contraction, so we take this value,  $\Omega_z$ , to characterize the initial rotation rate.

The initial rotation rate within a certain range does not significantly affect our results. For example, the rotating model with  $\Omega_z \simeq 20 \times 10^{-6} \text{ rad s}^{-1}$  can also reproduce the surface He, Li, and Be abundances of the Sun. However, this model has a faster rotating core than MBS22rt (see Figure 5), which appears inconsistent with helioseismic results. When the initial rotation rate  $\Omega_z$  reaches approximately  $30 \times 10^{-6} \text{ rad s}^{-1}$  ( $\approx 11 \Omega_\odot$ ), the model predicts not only a surface Li abundance lower than that advocated by

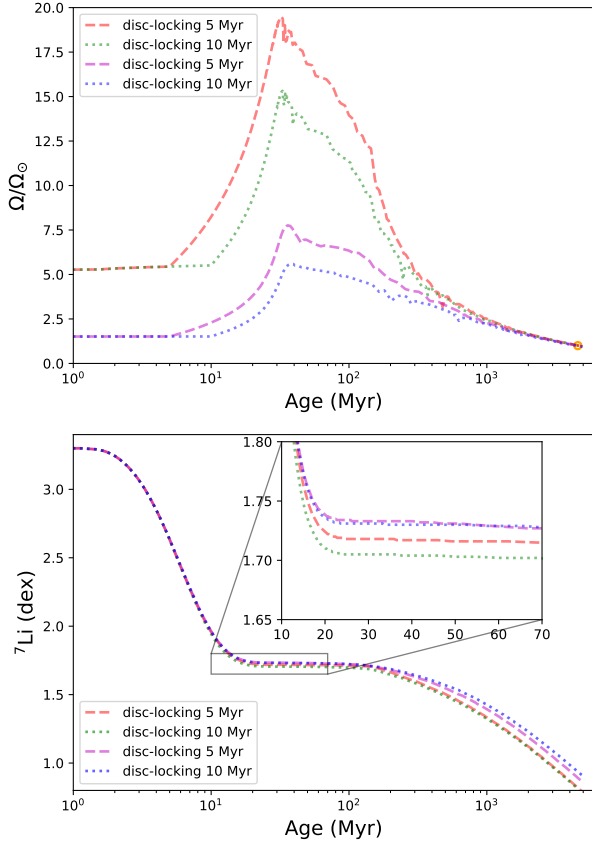


**Figure 6.** (a) Evolution of the surface angular velocity for  $1 M_\odot$  models with the same initial conditions except for initial velocities and disk lifetimes. These models are not calibrated to the Sun. (b) Evolution of the surface lithium abundance of these models.

E. X. Wang et al. (2021) but also an excessively fast core rotation. This occurs because the angular momentum stored in the Sun’s radiative region must be transferred to the CZ through the BCZ and then lost through the CZ. The more angular momentum stored at the ZAMS, the more intense the mixing at the BCZ during the MS, leading to excessive Li depletion, consistent with the calculations of J. P. Marques & M. J. Goupil (2013). Consequently, both helioseismic results and the observed Li abundance

seem to favor an initial solar rotation rate with  $\Omega_z < 10 \Omega_\odot$ , suggesting that the Sun might have been a slow rotator at the ZAMS rather than a fast rotator. However, this model does not align with observations of the Pleiades (J. Bouvier et al. 2018), where faster rotators exhibit less Li depletion.

The rotation rate  $\Omega_z$  depends on the initial rotation rate, disk-locking timescale, magnetic braking, and internal angular momentum transport. The evolution of surface rotation rate during the MS phase is primarily determined by the torque acting on the Sun and internal angular momentum transport. Although our models can reproduce the evolution of the surface rotation rates speculated from solar-type MS stars in clusters, the initial rotation rate during the pre-MS phase is lower than expected (see Figure 5).

In this work, we considered only the angular momentum loss mechanism of S. D. Kawaler (1988). It can reproduce the solar rotation rate at an age of 4.57 Gyr and the evolution of the surface rotation rates inferred from solar-type MS stars in clusters (see Figure 5). In addition to the S. D. Kawaler (1988) relation, other magnetic braking laws, such as those of A. Reiners & S. Mohanty (2012) and S. P. Matt et al. (2012, 2015), exist. These laws prescribe angular momentum loss rates that follow different power laws, which could affect the predicted Li and Be abundances. Therefore, Li and Be abundances may provide an opportunity to test these different formulas and the initial conditions of the Sun.

In our calculations, the value of  $f_c$  is 0.03. This is approximately consistent with the value of 0.046 adopted by M. H. Pinsonneault et al. (1989) and the 0.023 reported by I. Hunter et al. (2008) but it is significantly lower than the 0.8 suggested by V. Prat et al. (2016).

Angular momentum transport and material mixing in rotating models are dominated by



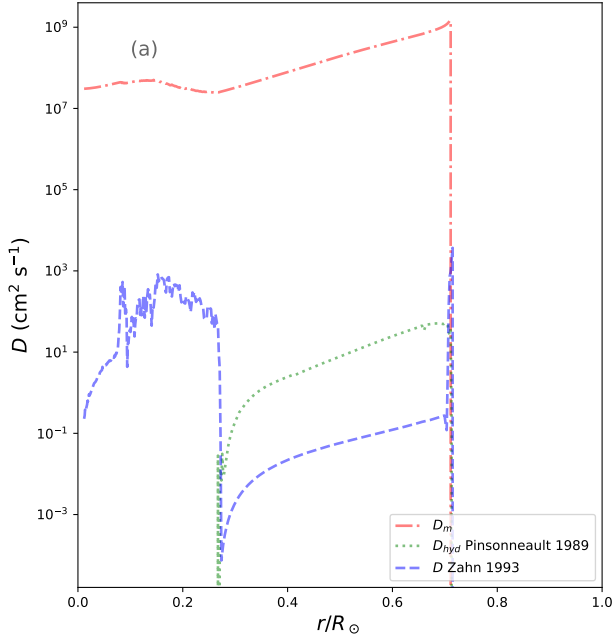


**Figure 7.** Hydrodynamic and magnetic diffusion coefficients as a function of radius for MBS22rt.

magnetic field effects. The magnetic diffusion coefficient is much larger than the hydrodynamic diffusion coefficients (see Figure 7). Solar models without magnetic fields cannot replicate the inferred nearly flat rotation profile in the radiative region (P. Eggenberger et al. 2022; W. Yang & Z. Tian 2024). The value of  $f_m$  is determined by both the inferred flat rotation profile and the observed Li and Be abundances. A slight decrease or increase in  $f_m$  necessitates a corresponding increase or decrease in  $f_{cm}$  to match the observed Li and Be abundances.

H. C. Spruit (2002) and A. Maeder & G. Meynet (2005) demonstrated that, when  $\omega_A \ll \Omega$ , where  $\omega_A$  is the Alfvén frequency, the coefficient for chemical transport is reduced by a factor  $(\omega_A/\Omega)^2$  compared to that for angular momentum transport. In our calculations, the parameter  $f_{cm}$  is assumed to be constant. The value of  $\omega_A/\Omega$  varies with radius and model age, ranging from approximately  $10^{-2}$  to  $10^{-4}$ , and is about  $10^{-2}$  at the BCZ.

The mixing efficiency in the CZ can also influence Li and Be abundances predicted by models. In our calculations, we determine the amounts of Li and Be consumed in each shell and assume that the material within the CZ is fully mixed instantaneously at each evolutionary time step.

Based on multidimensional simulations, I. Baraffe et al. (2017) proposed a new expression for the diffusion coefficient of overshooting. They assumed a maximum penetration depth,  $d_{ov}$ , that depends on the rotation rate, with fast rotation strongly limiting the vertical penetration of the convective plumes. Specifically, they set  $d_{ov} = 1 H_p$  if  $\Omega < 5 \Omega_\odot$  and  $0.1 H_p$  otherwise. Convective overshooting plays an important role in depleting Li during the pre-MS stage, as a larger overshooting distance results in a higher Li-burning rate in the overshooting region. K. C. Augustson & S. Mathis (2019) later modified this formula. In this work, we adopted the simplest classical treatment for convective overshoot.

Rotationally dependent overshooting has been used to explain the observed correlation between rotation and Li depletion in young clusters (I. Baraffe et al. 2017; T. Dumont et al. 2021a; T. Constantino et al. 2021). T. Dumont et al. (2021a) showed that, in addition to atomic diffusion, meridional circulation, and turbulent shear, additional parametric turbulent mixing processes are required to simultaneously explain the observed Li depletion and the solar rotational profile. However, this parametric turbulent mixing leads to a 0.3 dex depletion of Be by the age of the Sun, which is slightly too large compared to observations.

T. Constantino et al. (2021) demonstrated that fast rotation can suppress convection, thereby decreasing the temperature at the BCZ to an extent sufficient to account for the Li spread observed in young open clusters. The suppression effect is proportional to  $\Omega^2$  and, therefore, is not expected to be significant for

slow rotators. However, [T. Constantino et al. \(2021\)](#) did not consider microscopic diffusion, the reduction of effective gravity due to centrifugal force, or rotational mixing. If the suppression effect exists in the Sun, reproducing the seismically inferred convection depth would be more challenging. In this work, rotationally dependent overshooting and the suppression effect are not included. More studies are needed to fully understand the behavior of Li and Be in star clusters.

The settling of heavy elements has been confirmed by helioseismology, and thus, Be must undergo the gravitational settling. Only a portion of the Be deposited in the tachocline can be counteracted by rotational mixing, while most of it is transported to higher-temperature regions by settling, diffusion, and rotational mixing, where it is burned. Thus, the Be abundance predicted by a rotating model cannot be significantly higher than that predicted by the SSM MBS22. The maximum value of the surface Be abundance predicted by rotating models is 1.34 dex. This implies that [M. Asplund et al. \(2021\)](#) might have overestimated the solar surface Be abundance.

[M. H. Pinsonneault et al. \(1989\)](#) and [P. Eggenberger et al. \(2022\)](#) have shown that rotational mixing contributes to Li depletion in the Sun. The models of [W. Yang & Z. Tian \(2024\)](#) did not include the gravitational settling of Li and Be or the effect of tachocline, predicting a Li abundance higher than observed. Both [P. Eggenberger et al. \(2022\)](#) and our study considered the effects of magnetic fields. The rotation profiles in our models are similar to those of [P. Eggenberger et al. \(2022\)](#). However, their models predict a surface Be abundance lower than the observed value. If the gravitational settling of Li and Be is neglected in our calculations, our models can also reproduce the observed Li abundance but predict a Be abundance lower than observed. Neglecting the ef-

fect of the tachocline exacerbates these discrepancies. Additionally, the impact of accretion with varying abundances, which could explain the difference between Li and Be, is not considered in this work. The Li abundance predicted by the accretion models of [Q. S. Zhang et al. \(2019\)](#) is lower than observed, and they did not consider Be.

#### 4.2. Summary

In this work, we constructed standard and rotating solar models based on Magg’s mixtures. The surface helium abundance and the CZ depth of the SSM do not match the seismically inferred values. The surface Li abundance predicted by the SSM is inconsistent with the observed value.

To reproduce the helioseismic results and the observed Li abundance, the effects of rotation, magnetic fields, and gravitational settling must be considered. Consequently, we developed the rotating model, MBS22rt, which outperforms the SSM and the earlier rotating models, such as those in [P. Eggenberger et al. \(2022\)](#) and [W. Yang & Z. Tian \(2024\)](#). It assumes convective overshooting with  $\delta_{\text{ov}} = 0.09$  and a tachocline width of  $0.05R$ . MBS22rt exhibits superior sound speed and density profiles compared to the SSM and successfully reproduces the observed ratios  $r_{02}$  and  $r_{13}$ . The surface helium abundance and the CZ depth of MBS22rt are consistent with seismically inferred values within  $1\sigma$ . Furthermore, the fluxes of  $pp$ ,  $pep$ ,  $hep$ ,  ${}^7\text{Be}$ , and  ${}^8\text{B}$  neutrinos, as well as the total fluxes of  ${}^{13}\text{N}$ ,  ${}^{15}\text{O}$ , and  ${}^{17}\text{F}$  neutrinos, calculated from MBS22rt, agree with those reported by [J. Bergström et al. \(2016\)](#), [Borexino Collaboration \(2018\)](#), and [D. Basilio et al. \(2023\)](#) at the level of  $1\sigma$ .

Moreover, the rotating model predicts both a nearly flat rotation profile in the external part of the radiative region and an increase in the rotation rate in the solar core, which is in good agreement with that inferred from helioseismol-

ogy (M. J. Thompson et al. 2003; R. A. García et al. 2008). The surface Li abundance of 0.94 dex predicted by MBS22rt agrees with the value of  $0.96 \pm 0.05$  dex reported by E. X. Wang et al. (2021), while the surface Be abundance of 1.31 dex is consistent with  $1.32 \pm 0.05$  dex reported by S. Korotin & A. Kučinskas (2022). The rotating model can simultaneously reproduce the Sun's He, Li, and Be abundances, the seismically inferred CZ depth, the rotation profile, and other helioseismic results. This indicates that rotation, including magnetic fields, plays a key role in the evolution of the Sun. Since Li and Be have different physical properties, their depletion is governed by different physical mechanisms. The depletion of Be in the CZ of the Sun is dominated by gravitational settling but is affected by the tachocline and rotational mixing, whereas the depletion of Li in the CZ is mainly determined by convective overshooting and rotational mixing. The presence of the tachocline and rotational mixing accelerates the depletion

of Li abundance in the Sun but slows down Be depletion. These distinct depletion mechanisms result in the surface Li and Be evolving differently over time. The depletion of Li and Be also suggests that the helium abundance on the surface of the Sun has been enhanced by rotational mixing. An SSM with the correct metal abundance would underestimate the surface helium abundance.

Authors thank the anonymous referee for many useful suggestions that helped the authors significantly improve this work, as well as J. W. Ferguson for providing their low-temperature opacity tables, and acknowledge the support from the NSFC 11773005, 12222301, and the CSST Project. TZJ acknowledges the support from NSFC 11803030 and Yunnan Province Basic Research Program Project 202101AT070021.

## REFERENCES

- Ahmed, S. N., Anthony, A. E., Beier, E. W. et al. 2004, *PhRvL*, 92, 1301
- Asplund, M., Amarsi, A. M., Grevesse, N. 2021, *A&A*, 653, 141
- Augustson, K. C., & Mathis, S. 2019, *ApJ*, 874, 83
- Badnell, N. R., Bautista, M. A., Butler, K., et al. 2005, *MNRAS*, 360, 458
- Bahcall, J. N., & Pinsonneault, M. H. 1992, *RvMP*, 64, 885
- Bahcall, J. N., Pinsonneault, M. H., & Basu, S. 2001, *ApJ*, 555, 990
- Bahcall J. N., Pinsonneault M. H., & Wasserburg G. J. 1995, *RvMP*, 67, 781
- Balachandran, S. C., & Bell, R. A. 1998, *Nature*, 392, 791
- Baraffe, I., Pratt, J., Goffrey, T., et al. 2017, *ApJL*, 845, L6
- Basilico, D., Bellini, G., Benziger, J., et al. 2023, *PhRvD*, 108, 102005
- Basu, S., & Antia, H. M. 1997, *MNRAS*, 287, 189
- Basu, S., Chaplin, W. J., Elsworth, Y., New, R., & Serenelli, A. M. 2009, *ApJ*, 699, 1403
- Bellini, G. Benziger, J. Bick, D. et al. 2011, *PhRvL*, 107, 141302
- Bellini, G. Benziger, J. Bick, D. et al. 2012, *PhRvL*, 108, 51302
- Bergström, J., Gonzalez-Garcia, M. C., Maltoni, M., et al. 2016, *JHEP*, 3, 132
- Boesgaard, A. M., Armengaud, E, King, J. R. 2003a, *ApJ*, 582, 410
- Boesgaard, A. M., Armengaud, E, King, J. R. 2003b, *ApJ*, 583, 955
- Boesgaard, A. M., Armengaud, E, King, J. R. 2004, *ApJ*, 605, 864
- Boesgaard, A. M., Deliyannis, C. P., Lum, M. G., Chontos, A. 2022, *ApJ*, 941, 21
- Boesgaard, A. M., Lum, M. G., & Deliyannis, C. P. 2020, *ApJ*, 888, 28
- Bouvier, J., Lanzafame, A. C., Venuti, L., et al. 2016, *A&A*, 590, A78

- Bouvier, J., Barrado, D., Moraux, E., et al. 2018, *A&A*, 613, A63
- Böhm-Vitense, E. 1958, *ZAp*, 46, 108
- Borexino Collaboration ( Agostini, M., Altenmüller, K., Appel, S. et al.) 2018, *Nature*, 562, 505
- Appel, A., Bagdasarian, Z., Basilico, D., et al. 2022, *PhRvL*, 129, 252701
- Constantino, T., Baraffe, I., Goffrey, T., et al. 2021, *A&A*, 654, A146
- Chaboyer, B., Demarque, P., Pinsonneault, M. H. 1995, *ApJ*, 441, 865
- Chmielewski, Y., Brault, J. W., Mueller, E. A. 1975, *A&A*, 42, 37
- Chaplin, W. J., Elsworth, Y., Isaak, G. R., Miller, B. A., & New, R. 1999, *MNRAS*, 308, 424
- Charbonnel, C., & Talon, S. 2005, *Science*, 309, 2189
- Charbonneau, P., Christensen-Dalsgaard, J., Henning, R., et al. 1999, *ApJ*, 527, 445
- Christensen-Dalsgaard, J., Gough, D. O., & Thompson, M. J. 1991, *ApJ*, 378, 413
- Carlberg, J., Cunha, K., Smith, V. V., do Nascimento, J. D. 2018, *ApJ*, 865, 8
- Carlos, M., Meléndez, J., Spina, L., et al., 2019, *MNRAS*, 485, 4052
- Carlos, M., Meléndez, J., do Nascimento, J. D., & Castro, M. 2020, *MNRAS*, 492, 245
- Ding, M. Y., Shi, J. R., Yan, H. L., et al. 2024, *ApJS*, 271, 58
- Do Nascimento, J. D., Jr, Castro, M., Meléndez, J., et al. 2009, *A&A*, 501, 687
- Dumont, T., Charbonnel, C., Palacios, A., & Borisov, S. 2021a, *A&A*, 646, A48
- Dumont, T., Charbonnel, C., Palacios, A., & Borisov, S. 2021b, *A&A*, 654, A46
- Eff-Darwich, A., Korzennik, S. G., Jiménez-Reyes, S. J., & García, R. A. 2008, *ApJ*, 679, 1636
- Eggenberger, Haemmerlé, P., L., Meynet, G., Maeder, A. 2012, *A&A*, 539, A70
- Eggenberger, P., Buldgen, G., Salmon, S. J. A. J. 2019, *A&A*, 626, L1
- Eggenberger, P., Buldgen, G., Salmon, S. J. A. J., et al. 2022, *Nature Astronomy*, 6, 788
- Endal, A. S., & Sofia, S. 1976, *ApJ*, 210, 184
- Endal, A. S., & Sofia, S. 1978, *ApJ*, 220, 279
- Ferguson, J. W., Alexander, D. R., Allard, F. et al. 2005, *ApJ*, 623, 585
- Gallet, F., & Bouvier, J. 2015, *A&A*, 577, A98
- García, R. A., Mathur, S., Ballot, J. et al. 2008, *SoPh*, 251, 119
- García, R. A., Salabert, D., & Ballot, J. et al. 2011, *JPhCS*, 271, 012049
- Gálvez-Ortiz, M. C., Delgado-Mena, E., González Hernández, J. I., et al. 2011, *A&A*, 530, A66
- Greenstein, J. L., & Richardson, R. S. 1951, *ApJ*, 113, 536
- Greenstein, J. L., & Tandberg Hansen, E. 1954, *ApJ*, 119, 113
- Hunter, I., Brott, I., Lennon, D. J. et al. 2008, *ApJL*, 676, L29
- Iglesias, C., Rogers, F. J. 1996, *ApJ*, 464, 943
- Kawaler, S. D. 1988, *ApJ*, 333, 236
- Krishna Swamy, K. S. 1966, *ApJ*, 145, 174
- Korotin, S. & Kučinskas, A. 2022, *A&A*, 657, L11
- Kunitomo, M., & Guillot, T. 2021, *A&A*, 655, A51
- Kunitomo, M., Guillot, T., & Buldgen, G. 2022, *A&A*, 667, L2
- Lodders, K. 2021, *Space Science Reviews*, 217, 44
- Maeder, A., & Meynet, G. 2005, *A&A*, 440, 1041
- Magg, E., Bergemann, M., Serenelli, A., et al., 2022, *A&A*, 661, A140
- Marques, J. P., & Goupil, M. J. 2013, *LNP*, 865, 75
- Matt, S. P., MacGregor, K. B., Pinsonneault, M. H., & Greene, T. P. 2012, *ApJL*, 754, L26
- Matt, S. P., Brun, A. S., Baraffe, I., Bouvier, J., & Chabrier, G. 2015, *ApJ*, 799, L23
- Pietrow, A. G. M., Hoppe, R., Bergemann, M., Calvo, F. 2023, *A&A*, 672, L6
- Pinsonneault, M. H., Kawaler, S. D., Sofia, S., & Demarque, P. 1989, *ApJ*, 338, 424
- Prat, V., Guilet, J., Viallet, M., & Müller, E. 2016, *A&A*, 592, A59
- Reiners, A., & Mohanty, S. 2012, *ApJ*, 746, 43
- Rogers, F., & Nayfonov, A. 2002, *ApJ*, 576, 1064
- Roxburgh, I. W., & Vorontsov, S. V. 2003, *A&A*, 411, 215
- Seaton, M. J. 1987, *JPhB*, 20, 6363
- Smiljanic, R., Pasquini, L., & Randich, S. 2011, *A&A*, 535, A75
- Spruit, H. C. 2002, *A&A*, 381, 923
- Takeda, Y., Tajitsu, A., Honda, S., et al. 2011, *PASJ*, 63, 697
- Thompson, M. J., Christensen-Dalsgaard, J., Miesch, M. S., Toomre, J. 2003, *ARA&A*, 41, 599
- Thoul, A. A., Bahcall, J. N., Loeb, A. 1994, *ApJ*, 421, 828

- Turcotte, S., Richer, J., Michaud, G., Iglesias, C. A., & Rogers, F. J. 1998, *ApJ*, 504, 539
- Wang, E. X., Nordlander, T., Asplund, M., et al. 2021, *MNRAS*, 500, 2159
- Wang, E. X., Nordlander, T., Buder, S., et al. 2024, *MNRAS*, 528, 5394
- Xiong, D. R., & Deng, L. 2009, *MNRAS*, 395, 2013
- Yang, W. 2016, *ApJ*, 821, 108
- Yang, W. 2019, *ApJ*, 873, 18
- Yang, W. 2022, *ApJ*, 939, 61
- Yang, W. M., & Bi, S. L. 2006, *A&A*, 449, 1161
- Yang, W. M., & Bi, S. L. 2007, *ApJL*, 658, L67
- Yang, W., & Tian, Z. 2024, *ApJ*, 970, 38
- Zahn, J. P. 1993, in *Astrophysical Fluid Dynamics, Les Houches XLVII*, ed. J.-P. Zahn & J. Zinn-Justin (New York: Elsevier), 561
- Zhang, Q. S., Li, Y., Christensen-Dalsgaard, J. 2019, *ApJ*, 881, 103